Plasmonic gap-mode nanocavities with metallic mirrors in high-index cladding

Pi-Ju Cheng,[1,2] **Chen-Ya Weng,**[2,3] **Shu-Wei Chang,**[1,2,5] **Tzy-Rong Lin,**[3,4,*] **and Chung-Hao Tien**[1]

[1]*Department of Photonics, National Chiao Tung University, Hsinchu 30010, Taiwan*
[2]*Research Center for Applied Sciences, Academia Sinica, Nankang, Taipei 11529, Taiwan*
[3]*Institute of Optoelectronic Sciences, National Taiwan Ocean University, Keelung 20224, Taiwan*
[4]*Department of Mechanical and Mechatronic Engineering, National Taiwan Ocean University, Keelung 20224, Taiwan*
[5]*swchang@sinica.edu.tw*
[*]*trlin@ntou.edu.tw*

Abstract: We theoretically analyze plasmonic gap-mode nanocavities covered by a thick cladding layer at telecommunication wavelengths. In the presence of high-index cladding materials such as semiconductors, the first-order hybrid gap mode becomes more promising for lasing than the fundamental one. Still, the significant mirror loss remains the main challenge to lasing. Using silver coatings within a decent thickness range at two end facets, we show that the reflectivity is substantially enhanced above 95 %. At a coating thickness of 50 nm and cavity length of 1.51 μm, the quality factor is about 150, and the threshold gain is lower than 1500 cm^{-1}.

OCIS codes: (140.3410) Laser resonators; (240.6680) Surface plasmons; (230.7370) Waveguides; (250.5960) Semiconductor lasers; (260.3910) Metal optics.

References and links

1. J. A. Schuller, E. S. Barnard, W. Cai, Y. C. Jun, J. S. White, and M. L. Brongersma, "Plasmonics for extreme light concentration and manipulation," Nature Mater. **9**, 193–204 (2010).
2. M. T. Hill, "Status and prospects for metallic and plasmonic nano-lasers [invited]," J. Opt. Soc. B **27**, B36–B44 (2010).
3. R. M. Ma, R. F. Oulton, V. J. Sorger, and X. Zhang, "Plasmon lasers: coherent light source at molecular scales," Laser & Photon. Rev. **7**, 1–21 (2013).
4. M. Lončar, A. Scherer, and Y. Qiu, "Photonic crystal laser sources for chemical detection," Appl. Phys. Lett. **82**, 4648–4650 (2003).
5. Y. Nakayama, P. J. Pauzauskie, A. Radenovic, R. M. Onorato, R. J. Saykally, J. Liphardt, and P. Yang, "Tunable nanowire nonlinear optical probe," Nature **447**, 1098–1101 (2007).
6. R. G. Beausoleil, P. J. Kuekes, G. S. Snider, S. Y. Wang, and R. S. Williams, "Nanoelectronic and nanophotonic interconnect," Proc. IEEE **96**, 230–247 (2008).
7. M. T. Hill, Y. S. Oei, B. Smalbrugge, Y. Zhu, T. de Vries, P. J. van Veldhoven, F. W. M. van Otten, T. J. Eijkemans, J. P. Turkiewicz, H. de Waardt, E. J. Geluk, S. H. Kwon, Y. H. Lee, R. Nötzel, and M. K. Smit, "Lasing in metallic-coated nanocavities," Nat. Photonics **1**, 589–594 (2007).
8. M. T. Hill, M. Marell, E. S. P. Leong, B. Smalbrugge, Y. Zhu, M. Sun, P. J. van Veldhoven, E. J. Geluk, F. Karouta, Y. S. Oei, R. Nötzel, C. Z. Ning, and M. K. Smit, "Lasing in metal-insulator-metal sub-wavelength plasmonic waveguides," Opt. Express **17**, 11107–11112 (2009).
9. M. A. Noginov, G. Zhu, A. M. Belgrave, R. Bakker, V. M. Shalaev, E. E. Narimanov, S. Stout, E. Herz, T. Suteewong, and U. Wiesner, "Demonstration of a spaser-based nanolaser," Nature **460**, 1110–1112 (2009).
10. R. F. Oulton, V. J. Sorger, T. Zentgraf, R. M. Ma, C. Gladden, L. Dai, G. Bartal, and X. Zhang, "Plasmon lasers at deep subwavelength scale," Nature **461**, 629–632 (2009).

#185769 - $15.00 USD Received 22 Feb 2013; revised 6 May 2013; accepted 21 May 2013; published 29 May 2013

11. C. Y. Lu, S. W. Chang, S. L. Chuang, T. D. Germann, and D. Bimberg, "Metal-cavity surface-emitting microlaser at room temperature," Appl. Phys. Lett. **96**, 251101 (2010).
12. S. H. Kwon, J. H. Kang, C. Seassal, S. K. Kim, P. Regreny, Y. H. Lee, C. M. Lieber, and H. G. Park, "Subwavelength plasmonic lasing from a semiconductor nanodisk with silver nanopan cavity," Nano Lett. **10**, 3679–3683 (2010).
13. R. M. Ma, R. F. Oulton, V. J. Sorger, G. Bartal, and X. Zhang, "Room-temperature sub-diffraction-limited plasmon laser by total internal reflection," Nature Mater. **10**, 110–113 (2011).
14. R. A. Flynn, C. S. Kim, I. Vurgaftman, M. Kim, J. R. Meyer, A. J. Mäkinen, K. Bussmann, L. Cheng, F. S. Choa, and J. P. Long, "A room-temperature semiconductor spaser operating near 1.5 μm," Opt. Express **19**, 8954–8961 (2011).
15. M. J. H. Marell, B. Smalbrugge, E. J. Geluk, P. J. van Veldhoven, B. Barcones, B. Koopmans, R. Nötzel, M. K. Smit, and M. T. Hill, "Plasmonic distributed feedback lasers at telecommunications wavelengths," Opt. Express **19**, 15109–15118 (2011).
16. A. M. Lakhani, M. K. Kim, E. K. Lau, and M. C. Wu, "Plasmonic crystal defect nanolaser," Opt. Express **19**, 18237–18245 (2011).
17. C. Y. Wu, C. T. Kuo, C. Y. Wang, C. L. He, M. H. Lin, H. Ahn, and S. Gwo, "Plasmonic green nanolaser based on a metal-oxide-semiconductor structure," Nano Lett. **11**, 4256–4260 (2011).
18. K. J. Russell, T. L. Liu, S. Cui, and E. L. Hu, "Large spontaneous emission enhancement in plasmonic nanocavities," Nat. Photonics **6**, 459–462 (2012).
19. K. J. Russell and E. L. Hu, "Gap-mode plasmonic nanocavity," Appl. Phys. Lett. **97**, 163115 (2010).
20. C. Y. Lu, S. W. Chang, S. L. Chuang, T. D. Germann, U. W. Pohl, and D. Bimberg, "Low thermal impedance of substrate-free metal cavity surface-emitting microlasers," IEEE Photon. Technol. Lett. **23**, 1031–1033 (2011).
21. R. F. Oulton, V. J. Sorger, D. A. Genov, D. F. P. Pile, and X. Zhang, "A hybrid plasmonic waveguide for subwavelength confinement and long-range propagation," Nat. Photonics **2**, 496–500 (2008).
22. P. J. Cheng, C. Y. Weng, S. W. Chang, T. R. Lin, and C. H. Tien, "Cladding effect on hybrid plasmonic nanowire cavity at telecommunication wavelengths," IEEE J. Sel. Top. Quantum Electron. **19**, 4800306 (2013).
23. J. Grandidier, G. C. des Francs, S. Massenot, A. Bouhelier, L. Markey, J.-C. Weeber, C. Finot, and A. Dereux, "Gain-assisted propagation in a plasmonic waveguide at telecom wavelength," Nano Lett. **9**, 2935–2939 (2009).
24. D. Dai, Y. Shi, S. He, L. Wosinski, and L. Thylen, "Gain enhancement in a hybrid plasmonic nano-waveguide with a low-index or high-index gain medium," Opt. Express **19**, 12925–12936 (2011).
25. M. Ozeki, "Atomic layer epitaxy of III-V compounds using metalorganic and hydride sources," Mater. Sci. Rep. **8**, 97–146 (1992).
26. S. M. George, "Atomic layer deposition: an overview," Chem. Rev. **110**, 111–131 (2010).
27. D. P. Arnold, F. Cros, I. Zana, D. R. Veazie, and M. G. Allen, "Electroplated metal microstructures embedded in fusion-bonded silicon: conductors and magnetic materials," J. Microelectromech. Syst. **13**, 791–798 (2004).
28. S. W. Chang, T. R. Lin, and S. L. Chuang, "Theory of plasmonic Fabry-Perot nanolasers," Opt. Express **18**, 15039–15053 (2010).
29. A. Yariv and P. Yeh, *Optical Waves in Crystals* (Wiley and Sons, Hoboken, NJ, 1997).
30. P. B. Johnson and R. W. Christy, "Optical constants of the noble metals," Phys. Rev. B **6**, 4370–4379 (1972).
31. COMSOL Multiphysics, http://www.comsol.com.
32. S. Zhang and H. Xu, "Optimizing substrate-mediated plasmon coupling toward high-performance plasmonic nanowire waveguides," ACS Nano **6**, 8128–8135 (2012).
33. T. R. Lin, S. W. Chang, S. L. Chuang, Z. Zhang, and P. J. Schuck, "Coating effect on optical resonance of plasmonic nanobowtie antenna," Appl. Phys. Lett. **97**, 063106 (2010).
34. T. D. Visser, H. Blok, B. Demeulenaere, and D. Lenstra, "Confinement factors and gain in optical amplifiers," IEEE J. Quantum Electron. **33**, 1763–1766 (1997).
35. A. V. Maslov and C. Z. Ning, "Modal gain in a semiconductor nanowire laser with anisotropic bandstructure," IEEE. J. Quantum Electron. **40**, 1389–1397 (2004).
36. S. W. Chang and S. L. Chuang, "Fundamental formulation for plasmonic nanolasers," IEEE J. Quantum Electron. **45**, 1014–1023 (2009).
37. C. Y. Lu and S. L. Chuang, "A surface-emitting 3D metal-nanocavity laser: proposal and theory," Opt. Express **19**, 13225–13244 (2011).
38. C. Manolatou and F. Rana, "Subwavelength nanopatch cavities for semiconductor plasmon lasers," IEEE J. Quantum Electron. **44**, 435–447 (2008).
39. A. Mock, "First principles derivation of microcavity semiconductor laser threshold condition and its application to FDTD active cavity modeling," J. Opt. Soc. Am. B **27**, 2262–2272 (2010).

1. Introduction

There has been significant progress in miniaturized semiconductor lasers beyond the diffraction limit [1–3]. With advantages such as ultrasmall light spots and fast switching, plasmonic

#185769 - $15.00 USD Received 22 Feb 2013; revised 6 May 2013; accepted 21 May 2013; published 29 May 2013

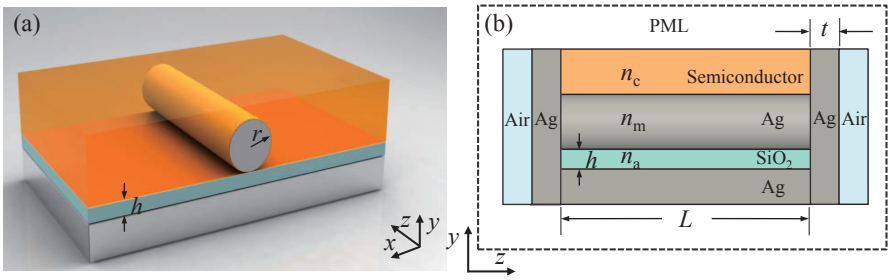

Fig. 1. (a) A metallic nanowire is separated from the Ag substrate by the active layer. The structure is embedded in a cladding layer. (b) The side view of the plasmonic gap-mode nanocavity. In practical calculations, the extended regions are surrounded by PMLs.

nanolasers have potential applications in biochemical sensing [4], imaging [5], and short-distance optical interconnects [6]. Despite the high loss accompanying the small cavity size achieved experimentally [7–19], metals may also serve as a multi-functional medium for reflectors, electrical injectors, and heatsinks [20]. Recently, Russell *et al*. have demonstrated a gap-mode plasmonic nanocavity consisting of a metallic nanowire and dielectric/metal planar structure [18, 19]. In analogy to the active dielectric nanowire [21, 22], the dielectric slab in their work can play the role of gain medium. Although metallic nanowires introduce the higher absorption than dielectric counterparts do, the experiment indicates that the cavity quality (Q) factor and threshold gain (g_{th}) of this type of cavities are mainly limited by the mirror loss at end facets rather than the propagation loss from metallic components [19].

In this paper, we analyze a three-dimensional (3D) plasmonic Fabry-Perot (FP) nanolaser based on surface-plasmon-polariton (SPP) gap modes at telecommunication wavelengths around 1.55 μm. The proposed configuration is composed of a truncated waveguide formed by a silver (Ag) nanowire and Ag substrate which sandwich a low-index dielectric gap of silicon dioxide (SiO_2), as indicated in Fig. 1(a). The dielectric gap plays the role of active regions and contains colloidal quantum dots (QDs) as the gain medium [23, 24]. The structure is covered by a thick cladding layer, and two Ag-coated end facets function as reflectors, as shown in Fig. 1(b). The refractive index n_c of the cladding will be varied in later calculations under different gap heights h and wire radii r. To model open regions outside two reflectors and extended cladding layers, we utilize perfectly matched layers (PMLs) around the cavity for practical calculations. We are particularly interested in the case of $n_c = 3.5$ because it corresponds to the deposition of semiconductors as the cladding layer. In this way, the technologies of silicon photonics and microelectronics, including group-IV and III-V semiconductors [25–27], may be further integrated with plasmonics and bring about more functionalities.

A high cladding refractive index, nevertheless, affects the characteristics of lasing modes. In fact, the cross-sectional profile of the FP lasing mode at a low cladding index is not identical to that at a high index. The fundamental transverse mode of the guiding structure in Fig. 1 is the most promising for lasing at a low cladding index [22]. In the high-index condition, however, the first-order mode often exhibits the better field confinement in the active region than the fundamental one does. Thus, rather than the fundamental guided mode which is usually the focus in typical FP cavities, we look into the first-order mode in the presence of high-index cladding materials such as semiconductors.

The mirror loss is responsible for the low Q factor and high threshold gain in this type of cavities [18, 19]. Rather than prolonging the FP cavity to decrease the mirror loss, an alternative solution is to increase the reflectivity. We utilize interference patterns between the incident

#185769 - $15.00 USD Received 22 Feb 2013; revised 6 May 2013; accepted 21 May 2013; published 29 May 2013

mode and reflected field (standing waves) [28] and the orthogonality theorem of waveguide modes [29] to calculate the modal reflection coefficient and reflectivity of Ag mirrors. The result indicates that Ag mirrors can reach a reflectivity above 95 % with the coating thickness t of about a few ten nanometers. The corresponding threshold reduction makes the lasing action at a shorter cavity length L potentially sustainable with colloidal QDs [23, 24].

The remaining part of the paper is organized as follows. In section 2, we use the two-dimensional (2D) finite-element method (FEM) to compare characteristics of the fundamental and first-order SPP gap modes. We then utilize the orthogonality theorem of waveguide modes and 3D FEM to extract the modal reflectivity and show how it increases with the coating thickness in section 3. In section 4, we use the FP round-trip oscillation condition to estimate the required cavity length, Q factor, and threshold gain so that the lasing action at the target wavelength of 1.55 μm is permissible. We conclude our discussions in section 5.

2. Analysis of modal characteristics

The SPP gap modes of the cavity structure in Fig. 1 are formed by the coupling between plasmonic modes of the circular Ag nanowire and surface waves of the active layer sandwiched by the Ag substrate and cladding. The coupling strengths between these two categories of modes are sensitive to variations of parameters such as the cladding index n_c, gap height h, and wire radius r [21]. Depending on the parameters, the features of one type of modes may dominate those of the other type and vice versa. In the following analysis, we set the refractive index n_m of Ag to $0.16+11.09i$ [30] and counterpart n_a of SiO_2 to 1.5 at the wavelength of 1.55 μm. Calculations are conducted with the 2D FEM eigenmode solver of the software COMSOL [31].

When a circular metallic cylinder (Ag nanowire in the cavity structure of interest) is adjacent to a dielectric gap layer atop the metallic substrate, the rotational symmetry is broken, and guided modes of the cylinder are strongly coupled to surface plasmon modes localized near/within the dielectric gap through evanescent fields from the two parts. This coupling leads to plasmonic gap modes in the composite guiding structure. For the circular metallic cylinder in a homogeneous dielectric, the TM_0 guided mode (azimuthal mode number $m = 0$) is a non-cutoff, circularly symmetric one with the maximal field strength localized around the circumference. On the other hand, the two degenerate first-order modes $HE_{\pm 1}$ ($m = 1$) on the circular cross section correspond to parallel ($+1$) and normal (-1) free charge oscillations to the planar structure [32]. As the metallic cylinder is in the proximity to a flat plane, the guided modes TM_0 and HE_{-1} are hybridized and mixed with gap modes of the planar structure. For the whole guiding structure, if there is considerable field strength distributed in the cladding, the fundamental hybrid gap mode exhibits characteristics of the TM_0 mode, while the first-order one carries features of the HE_{-1} mode with a dominant field normal to the planar structure.

In Fig. 2, we show square magnitudes $|\mathbf{E}(\boldsymbol{\rho})|^2$ of the cross-sectional profiles ($\boldsymbol{\rho} = x\hat{x} + y\hat{y}$ is the transverse coordinate) for the fundamental and first-order modes at $h = 10$ nm, $r = 70$ nm, and $n_c = 1,\ 2.5$ and 3.5. The corresponding effective indices are $2.24 + 0.014i$ [inset in Fig. 2(a)], $3.31 + 0.020i$, $4.10 + 0.022i$, $2.55 + 0.004i$, and $3.54 + 0.018i$ [Fig. 2(a) to (d)], respectively. From the inset in Fig. 2(a), the fundamental mode at $n_c = 1$ ($< n_a = 1.5$) is localized near the bottom of the nanowire, which is similar to the localized field near tips of metallic bowtie structures [33]. The localized field below the wire bottom does not penetrate into the active region much. At $n_c = 2.5$ [Fig. 2(a)], in contrast, the field of the fundamental hybrid gap mode is tightly confined in the active region below the nanowire and does not spread around lossy regions of the Ag nanowire and substrate. Such an advantage for lasing is, nevertheless, absent in the target case of $n_c = 3.5$ (semiconductors) because the nature of TM_0 mode emerges on the mode profile, as can be observed from the field strength which is quite circularly symmetric near the nanowire in Fig. 2(b). Under such circumstances, the poorer field confinement

#185769 - $15.00 USD Received 22 Feb 2013; revised 6 May 2013; accepted 21 May 2013; published 29 May 2013

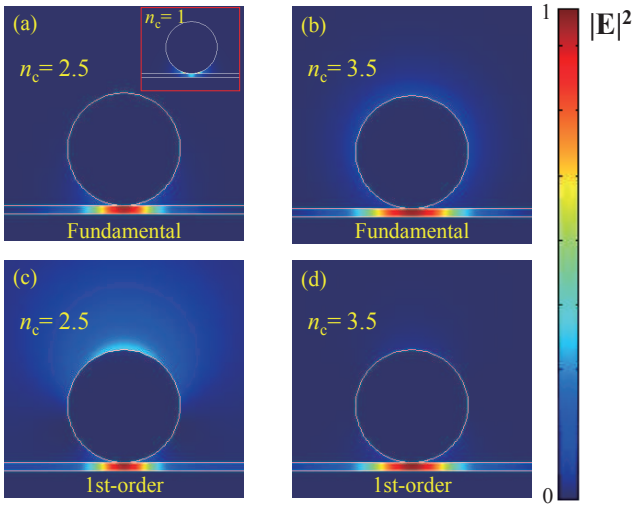

Fig. 2. Square magnitudes $|\mathbf{E}(\boldsymbol{\rho})|^2$ of the cross-sectional profiles for the fundamental mode at (a) $n_c = 2.5$ (inset: $n_c = 1$) and (b) $n_c = 3.5$, and for the first-order mode at (c) $n_c = 2.5$ and (d) $n_c = 3.5$. The height h and radius r are 10 and 70 nm, respectively. At $n_c = 3.5$, the first-order mode is better confined in the active region than the fundamental one is.

in the active region and more significant distribution around the Ag nanowire makes the fundamental mode less promising for lasing in the presence of semiconductor claddings.

The field evolution of the first-order mode proceeds with a reverse trend to that of the fundamental one as n_c increases. At $n_c \leq n_a$, the first-order mode is a leaky one with the majority of the field distributed in the free space outside the Ag nanowire, dielectric gap, and substrate. As soon as $n_c > n_a$, the mode begins to localize around the Ag nanowire and active region. From Fig. 2(c), the nature of HE_{-1} modes at $n_c = 2.5$ is reflected on the field partially distributed near the *upper half* of the nanowire and within the active region. On the other hand, from Fig. 2(d), at $n_c = 3.5$, the feature of HE_{-1} modes becomes much more prominent. The lower lobe of HE_{-1} modes closely overlaps with the gap mode of the planar structure. Accordingly, at this cladding index, the first-order mode is tightly confined inside the active gap, which is promising for lasing. Therefore, if we would pick up a cross-sectional profile for the lasing mode with semiconductor claddings, the first-order mode should be the choice.

Evolutions of different modes as n_c changes are more easily understood from the waveguide confinement factor Γ_{wg} and modal loss α_i which are relevant to lasing. The waveguide confinement factor Γ_{wg} is defined as the ratio between the modal gain and material gain in the active region. Its expression is written as [34–36]

$$\Gamma_{wg} = \frac{\frac{n_a}{2\eta_0}\int_{A_a} d\boldsymbol{\rho}\,|\mathbf{E}(\boldsymbol{\rho})|^2}{\int_A d\boldsymbol{\rho}\frac{1}{2}\mathrm{Re}\left[\mathbf{E}(\boldsymbol{\rho})\times\mathbf{H}^*(\boldsymbol{\rho})\right]\cdot\hat{z}}, \tag{1}$$

where η_0 is the intrinsic impedance; A_a is the cross section of the active region; A is the whole cross section ideally extending to the infinity; and $\mathbf{H}(\boldsymbol{\rho})$ is the cross-sectional magnetic-field profile of the guided mode. Note that the denominator in Eq. (1) is the total power flow of the guided mode while the numerator also bears a similar feature as if the mode were a plane wave in the active region. In some cases such as guided modes with low group velocities, the numerator in Eq. (1) can be larger than the denominator [34–36]. Under such circumstances, the

#185769 - $15.00 USD Received 22 Feb 2013; revised 6 May 2013; accepted 21 May 2013; published 29 May 2013

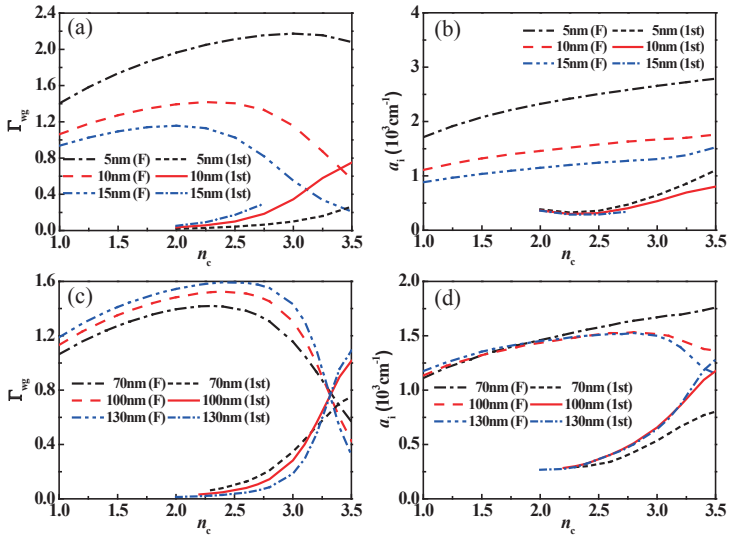

Fig. 3. (a) The waveguide confinement factor Γ_{wg} and (b) modal loss α_i of the fundamental and first-order hybrid gap modes versus n_c at different $h = 5$, 10, and 15 nm and a fixed $r =$ 70 nm. (c) and (d) are the counterparts of (a) and (b) at a fixed $h = 10$ nm and different $r =$ 70, 100, and 130 nm. Symbols "F" and "1st" indicate fundamental and first-order modes, respectively.

parameter Γ_{wg} is over unity and should be regarded as a conversion ratio rather than confinement factor. As to the modal loss α_i, it can be obtained from the imaginary part of the modal propagation constant k_z as $\alpha_i = 2\mathrm{Im}[k_z]$, which is numerically calculated with 2D FEM. Its inverse α_i^{-1} describes how long the mode can propagate in a waveguide.

Behaviors of the waveguide confinement factor Γ_{wg} and modal loss α_i are influenced by the group velocity $v_{g,z}$ of the guided mode, which is a characteristic of the energy flow and is expressed as $[\partial \mathrm{Re}[k_z]/\partial\omega]^{-1}$. In addition, the parameters Γ_{wg} and α_i are also proportional to the overlaps of fields with the active and lossy regions, respectively. In fact, we can write $\Gamma_{wg} \propto v_{g,z}^{-1}\int_{A_a} \mathrm{d}\boldsymbol{\rho}|\mathbf{E}(\boldsymbol{\rho})|^2$ and $\alpha_i \propto v_{g,z}^{-1}\int_{A_m} \mathrm{d}\boldsymbol{\rho}|\mathbf{E}(\boldsymbol{\rho})|^2$, where A_m is the cross section of the metal region [36]. From these relations, the ratio α_i/Γ_{wg} only depends on the field strengths in the gain and lossy regions and is therefore free from the disguise of the group velocity $v_{g,z}$. The physical meaning of this ratio will be discussed later.

The waveguide confinement factor Γ_{wg} and modal loss α_i of the fundamental and first-order modes as a function of the cladding index n_c at different gap heights $h = 5$, 10, and 15 nm and a fixed wire radius $r = 70$ nm are shown in Fig. 3(a) and (b), respectively. The counterparts at a fixed height $h = 10$ nm and different radii $r = 70$, 100, and 130 nm are shown in Fig. 3(c) and (d). Due to the wide-spreading field of the weakly guided first-order mode in the cladding when n_c is not sufficiently larger than $n_a = 1.5$, we start calculations at $n_c = 2$ for this mode since the outcome may be affected by interferences from boundaries of the computation domain. For the first-order mode, we also skip the calculations at large gap heights because the feature of the slowly-decreasing HE_{-1} mode in the open region also appear on the hybrid field profile at $h > 12$ nm. From Fig. 3(a) and (b), the gap height h has a significant impact on Γ_{wg} and α_i of the fundamental mode. Both parameters of this mode are enhanced by the lower group velocity $v_{g,z}$ of the fundamental mode at the smaller h and smaller n_c while the more field distribution in metallic regions additionally increases α_i. On the other hand, the two parameters

#185769 - $15.00 USD Received 22 Feb 2013; revised 6 May 2013; accepted 21 May 2013; published 29 May 2013

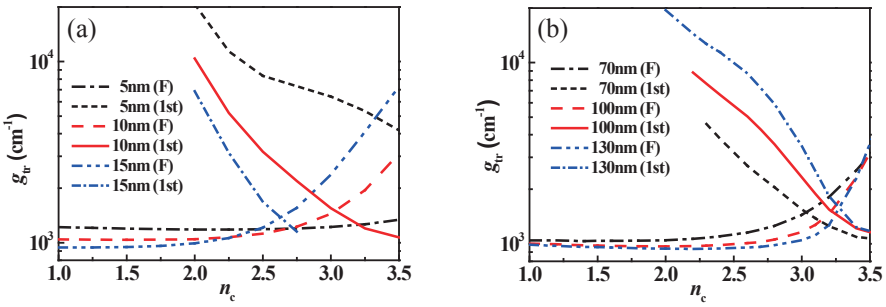

Fig. 4. Transparency gains g_{tr} of the fundamental and first-order hybrid gap modes at (a) different $h = 5$, 10, and 15 nm and a fixed $r = 70$ nm, and (b) different $r = 70$, 100, and 130 nm and a fixed $h = 10$ nm. Symbols "F" and "1st" indicate fundamental and first-order modes, respectively.

of the first-order mode exhibit quite distinct dependence on h to that of the fundamental mode. The waveguide confinement factor of the first-order mode becomes lower at the smaller h while the modal loss does not alter as significantly. At a large n_c, it is the field distribution rather than the group velocity that governs these two parameters for both modes. At the smaller h, the distributions of the first-order mode in the cladding is slightly increased, but the counterpart in the active region is much reduced. As a result, the corresponding waveguide confinement factor is much lower, but the modal loss becomes larger mildly at the smaller h.

The trends of Γ_{wg} and α_i as n_c varies are also different between the two modes and are directly related to the corresponding mode profiles in Fig. 2. As n_c increases from unity to 3.5, the confinement factors Γ_{wg} of the fundamental mode first increase mildly but then decrease wildly, at which the counterparts of the first-order mode grow sharply. For each pair of curves with the same gap height h in Fig. 3(a), there seems to be a connection between the drop of Γ_{wg} for the fundamental mode and growth of the counterpart for the first-order one as n_c increases, indicating that the mixing between the TM_0 and HE_{-1} modes of the Ag nanowire should be present in addition to the coupling to SPP waves of the planar structure. Other than that, the behavior of Γ_{wg} versus n_c for the fundamental mode just reflects the field evolution in Fig. 2(a) and (b), and the enhancement of Γ_{wg} for the first-order mode corresponds to the increasing portion of the field inside the active region, as shown in Fig. 2(c) and (d). While the variation of α_i with n_c is relatively mild for the fundamental mode, the increase of this parameter for the first-order mode is due to the accompanying penetration into the Ag substrate when the field is more confined in the active region.

The behaviors of Γ_{wg} and α_i versus n_c for different radii r and a fixed gap height h in Fig. 3(c) and (d) are analogous to those in Fig. 3(a) and (b). However, the effect of the wire radius r is less significant than that of the gap height h, as can be observed from quantitatively similar curves in Fig. 3(c) and (d).

A critical parameter as viewed from points of the lasing threshold is the necessary material gain which sustains the propagation of the mode *without being attenuated*. This gain is denoted as the transparency threshold g_{tr}, which is one portion of the threshold gain g_{th} in addition to the other component compensating the mirror loss of FP lasers. The transparency condition $\alpha_i - \Gamma_{wg} g_{tr} = 0$ directly gives rise to the expression of transparency threshold as $g_{tr} = \alpha_i / \Gamma_{wg}$. It is usually desired to minimize g_{tr} under given constraints of guiding structures. In Fig. 4(a) and (b), we show the transparency threshold gains g_{tr} of the fundamental and first-order modes corresponding to Fig. 3(a) and (b) as well as 3(c) and (d), respectively. Note that as mentioned

#185769 - $15.00 USD Received 22 Feb 2013; revised 6 May 2013; accepted 21 May 2013; published 29 May 2013

earlier, the effect of group velocity $v_{g,z}$ on Γ_{wg} and α_i is absent in g_{tr}, and the information of the field distributions in the active region and metallic areas is clearer in g_{tr} than in Γ_{wg} and α_i.

From Fig. 4(a), the transparency thresholds of the fundamental mode at the smaller h are higher at the low-n_c side, but the opposite trend occurs at the other side. This unexpected phenomenon is due to the fact that the field inside the thicker active region is more easily drawn into the cladding at a high index n_c. On the other hand, reflecting the more portion of the field inside the active region than in the cladding and Ag substrate, the transparency threshold of the first-order mode is lower at the larger h. In general, the transparency threshold g_{tr} of the fundamental mode and that of the first-order one increases and decreases with n_c, respectively, which indicates that different modes should be adopted for lasing in distinct ranges of n_c. From Fig. 4(b), the transparency thresholds g_{tr} of these two modes as a function of n_c at different radii follow similar trends to those in Fig. 4(a). The nanowire radius r, on the other hand, does not dramatically and quantitatively alter the magnitude of g_{tr}.

At $n_c = 3.5$ (semiconductors), the transparency threshold of the first-order mode is usually lower than that of the fundamental one unless the gap height h is extremely narrow [for example, $h = 5$ nm in Fig. 4(a)]. At this stage, to minimize the propagation loss from the metal absorption in the presence of semiconductor claddings, the first-order transverse mode of this plasmonic waveguide should be the target mode. In the following calculations, we will therefore focus on threshold characteristics of the first-order mode.

3. Mirror reflectivity

The mirror loss is another factor hindering the lasing action of the plasmonic nanolaser. As the cavity length L of the FP cavity is shortened, the power leakage from two end facets is enhanced. In fact, with a cavity length L in the (sub)micron range, the mirror loss can easily dominate the propagation loss, and increasing the reflectivity becomes necessary for the threshold reduction. For this purpose, we consider Ag coatings of a few tens of nanometers at two end facets of the plasmonic cavity as reflectors.

The lasing mode of a FP cavity may be approximated as the standing wave corresponding to one specific transverse guided mode since the cavity resonance is mainly attributed to it. On the other hand, other modes of the guiding structure, no matter guided, leaky, or evanescent ones, may be present in the lasing mode since boundary conditions of fields at waveguide/mirror junctions need to be satisfied (mode matching). The transmissions, reflections, and scattering of all waveguide modes at those junctions couple to each other. Their effects on the power reflectivity are not easily modeled because modal reflections and constituents of all the waveguide modes in the FP cavity have to be self-consistently determined.

Here, we adopt a simplified approach by sending an incident wave merely composed of the main guided mode at resonance onto the mirror and analyze the resulted reflected/total field. The reflected field contains many backward-propagating/evanescent components in addition to the one corresponding to the incident wave. We use the orthogonality theorem of waveguide modes [29] to extract the backward-propagating amplitude corresponding to the main guided mode. The ratio between this backward-propagating amplitude and that of the incident wave is adopted as an estimation of the reflection coefficient. The effect from other nonresonant components is assumed minor, which is often valid when the resonance exhibits a decently narrow spectral linewidth.

The orthogonality theorem of modes in a waveguide consisting of isotropic materials reads as follows [29]:

$$\int_A \mathrm{d}\boldsymbol{\rho}[\mathbf{E}_{l'}(\boldsymbol{\rho}) \times \mathbf{H}_l(\boldsymbol{\rho})] \cdot \hat{z} = \int_A \mathrm{d}\boldsymbol{\rho}[\tilde{\mathbf{E}}_{l'}(\boldsymbol{\rho}) \times \mathbf{H}_l(\boldsymbol{\rho})] \cdot \hat{z} = \delta_{l'l}\Lambda_l, \tag{2}$$

#185769 - $15.00 USD Received 22 Feb 2013; revised 6 May 2013; accepted 21 May 2013; published 29 May 2013

where $\mathbf{E}_{l'}(\boldsymbol{\rho})$ and $\mathbf{H}_l(\boldsymbol{\rho})$ are the cross-sectional electric and magnetic field profiles of modes l' and l, respectively; $\tilde{\mathbf{E}}_{l'}(\boldsymbol{\rho})$ is the backward-propagating/evanescent counterpart of $\mathbf{E}_{l'}(\boldsymbol{\rho})$; $\delta_{l'l}$ is the Kronecker delta; and Λ_l is a normalization constant. Note that conventionally, the form of $\tilde{\mathbf{E}}_{l'}(\boldsymbol{\rho})$ is chosen so that it has transverse ($\perp \hat{z}$) and longitudinal ($\| \hat{z}$) components identical and opposite in signs to those of $\mathbf{E}_{l'}(\boldsymbol{\rho})$, respectively. We consider an incident wave entirely composed of the main resonant guided mode l of the FP cavity, namely,

$$\mathbf{E}_{\mathrm{inc}}(\mathbf{r}) = F_l \mathbf{E}_l(\boldsymbol{\rho}) e^{ik_{z,l}z}, \tag{3}$$

where F_l and $k_{z,l}$ are the forward-propagating amplitude and propagation constant of mode l, respectively; and the origin of the coordinate z is set at the waveguide/mirror junction. In addition to $\mathbf{E}_{\mathrm{inc}}(\mathbf{r})$, the total field $\mathbf{E}_{\mathrm{tot}}(\mathbf{r}) = \mathbf{E}_{\mathrm{inc}}(\mathbf{r}) + \mathbf{E}_{\mathrm{r}}(\mathbf{r})$ at $z < 0$ also contains the reflected field $\mathbf{E}_{\mathrm{r}}(\mathbf{r})$, which can be expanded with backward-propagating/evanescent modes as

$$\mathbf{E}_{\mathrm{r}}(\mathbf{r}) = \sum_{l'} B_{l'} \tilde{\mathbf{E}}_{l'}(\boldsymbol{\rho}) e^{-ik_{z,l'}z}. \tag{4}$$

With the expression of $\mathbf{E}_{\mathrm{inc}}(\mathbf{r})$ in Eq. (3), 3D FEM, and a sufficient number of waveguide modes (five in this case) taken into account, the total field $\mathbf{E}_{\mathrm{tot}}(\mathbf{r})$ is numerically calculated.

Our goal is to extract the reflection coefficient of mode l defined as $r_{\mathrm{m}} = B_l/F_l$ from the information of $\mathbf{E}_{\mathrm{tot}}(\mathbf{r})$ and the magnetic cross-sectional profile $\mathbf{H}_l(\boldsymbol{\rho})$. Using the orthogonality theorem in Eq. (2) and generalizing the approach in Ref. [28], we integrate the quantity $[\mathbf{E}_{\mathrm{tot}}(\mathbf{r}) \times \mathbf{H}_l(\boldsymbol{\rho})] \cdot \hat{z}$ over the whole waveguide region A at $z < 0$ to eliminate amplitudes other than F_l and B_l and denote the outcome as a function $f(z)$:

$$\int_A \mathrm{d}\boldsymbol{\rho} [\mathbf{E}_{\mathrm{tot}}(\mathbf{r}) \times \mathbf{H}_l(\boldsymbol{\rho})] \cdot \hat{z} \equiv f(z) = \Lambda_l \left(F_l e^{ik_{z,l}z} + B_l e^{-ik_{z,l}z} \right) = C \left(e^{ik_{z,l}z} + r_{\mathrm{m}} e^{-ik_{z,l}z} \right), \tag{5}$$

where C is the product $\Lambda_l F_l$. The magnitude $|f(z)|$ at $z < 0$ exhibits an interference pattern of standing waves as follows:

$$|f(z)| = |C| \sqrt{e^{-2\mathrm{Im}[k_{z,l}]z} + |r_{\mathrm{m}}|^2 e^{2\mathrm{Im}[k_{z,l}]z} + 2|r_{\mathrm{m}}| \cos\left(2\mathrm{Re}[k_{z,l}]z - \theta_r\right)}, \tag{6}$$

where θ_r is the phase angle of r_{m}. The form of $|f(z)|$ in Eq. (6) is utilized as a model function in the least squares fitting to the absolute value of the numerical integration at the left-hand side of Eq. (5). The magnitudes $|C|$ and $|r_{\mathrm{m}}|$ and phase angle θ_r are taken as three fitting parameters, and the value of $|r_{\mathrm{m}}|$ which optimizes the fitting is used to estimate the reflectivity $R = |r_{\mathrm{m}}|^2$ of the target FP mode.

In Fig. 5, we show the reflectivity of the first-order mode versus the thickness t of the Ag mirror at $h = 10$ nm, $r = 70$ nm, and $n_{\mathrm{c}} = 3.5$. From Fig. 5, without the Ag mirror ($t = 0$ nm), the reflection is completely due to the waveguide/air interface, and the corresponding reflectivity is 50.6 %. This reflectivity may bring about an enormous mirror loss and deteriorate the lasing performance if the cavity is short. On the other hand, Ag coatings of a few ten nanometers dramatically enhance the reflectivity. In the inset of Fig. 5, we show the standing-wave pattern $|f(z)|$ and corresponding least-square fitting at $t = 50$ nm. The effective index of the guided mode defined as $n_{\mathrm{eff}} = k_z/k_0$, where k_0 is the vacuum propagation constant at the target wavelength of 1.55 μm, is $3.49 + 0.011i$. The effective index n_{eff} (k_z) determines the oscillation and decay/growth of the interference pattern. If the thickness t is more than 25 nm, the reflectivity R can be higher than 90 % ($R = 90.4$ % at t=25 nm). At $t = 50$ nm, the result indicates $|r_{\mathrm{m}}| = 0.978$ ($R = 95.7$ %) and $\theta_r = 1.180\pi$. We note that the reflectivity calculated from simple Fresnel's formula using the effective index n_{eff} and refractive index n_{m} of Ag deviates significantly from the estimation here due to the invalid approximation of plane-wave incidences.

#185769 - $15.00 USD Received 22 Feb 2013; revised 6 May 2013; accepted 21 May 2013; published 29 May 2013

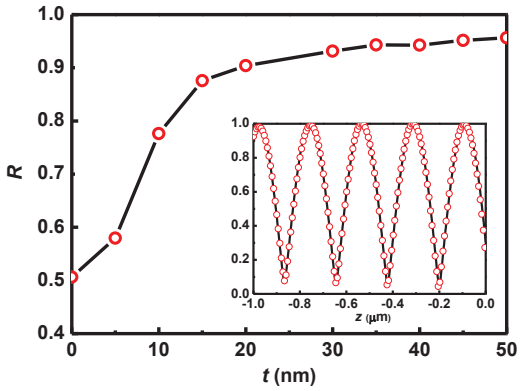

Fig. 5. The reflectivity R of the first-order mode as a function of the Ag thickness t at $h = 10$ nm, $r = 70$ nm, and $n_c = 3.5$. Without the mirror, the reflectivity is about 50 %. As $t > 25$ nm, the reflectivity can exceed 90 %. The inset is the standing-wave pattern $|f(z)|$ (circle marks) and its fitting (solid line) at $t = 50$ nm ($R = 95.7$ %).

The mirror loss is quite significant if the nanocavity has a cavity length L as short as few micrometers. Under such circumstances, the threshold gain is dominated by the mirror loss rather than modal loss. Thickening Ag reflectors is an efficient way to enhance the reflectivity and provides a solution to the high threshold. On the other hand, the high reflectivity also leads to a poor output power efficiency [37] because most of the generated power is blocked inside the cavity and dissipated as heat. This trade-off between threshold gain and output power should be taken into account in the choice of the reflector thickness t.

4. Estimations from Fabry-Perot formulae and three-dimensional mode pattern

The remaining issue of the plasmonic FP cavity, in addition to the modal characteristics (Γ_{wg}, α_i, and g_{tr}) and reflection coefficient r_m (reflectivity R), is the cavity length L. This length has to be carefully chosen so that the mirror loss is decently low while the resonance around the target wavelength of 1.55 μm is supported.

We first look into the quality factor Q_{FP} and threshold gain $g_{th,FP}$ of the FP cavity based on the round-trip oscillation condition:

$$\frac{1}{Q_{FP}} = \frac{1}{Q_{abs}} + \frac{1}{Q_{mir}}, \tag{7a}$$

$$\frac{1}{Q_{abs}} = \frac{v_{g,z}\alpha_i}{\omega_r}, \quad \frac{1}{Q_{mir}} = \frac{v_{g,z}\alpha_{mir}}{\omega_r}, \quad \alpha_{mir} = \frac{1}{L}\ln\left(\frac{1}{R}\right), \tag{7b}$$

$$g_{th,FP} = \frac{\alpha_i + \alpha_{mir}}{\Gamma_{wg}}, \tag{7c}$$

where the Q factor components Q_{abs} and Q_{mir} originate from the modal loss α_i and mirror loss α_{mir}, respectively; ω_r is the resonance frequency corresponding to the wavelength of 1.55 μm. From Eq. (7b) and (7c), the cavity length L needs to be sufficiently long in order to lower α_{mir} and $g_{th,FP}$. This requirement does not always coincide with the goal of ultrasmall sizes. In addition to this constraint, only specific cavity lengths L satisfy the round-trip phase condition of the FP cavity at the target wavelength of 1.55 μm:

$$2\mathrm{Re}[k_z]L + 2\theta_r = 2m\pi, \quad m \in \mathbb{N}, \tag{8}$$

#185769 - $15.00 USD Received 22 Feb 2013; revised 6 May 2013; accepted 21 May 2013; published 29 May 2013

Table 1. The reflectivities, quality factors, and threshold gains of cavity modes corresponding to mirror thicknesses $t = 0$ ($L = 660$ and 1547 nm) and 50 nm ($L = 625$ and 1511 nm) at the wavelength of 1.55 μm. The cavity parameters are set as follows: $h = 10$ nm, $r = 70$ nm, and $n_c = 3.5$.

t (nm)	L (nm)	R	Γ_{wg}	$g_{th,FP}$ (cm^{-1})	Q_{abs}	Q_{mir}	Q_{FP}
0	660	0.506	0.734	15127.0	206.0	15.7	14.6
	1547			7071.4		36.8	31.2
50	625	0.957		2041.4		227.6	108.2
	1511			1472.5		550.6	149.9

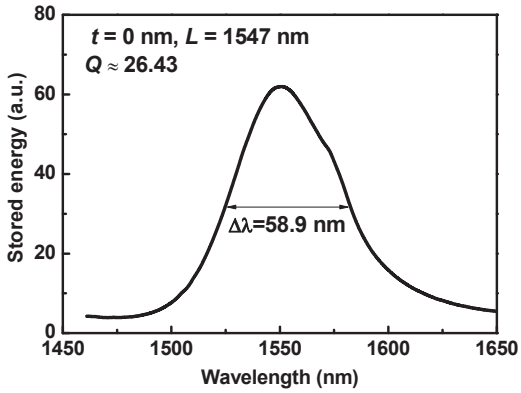

Fig. 6. The resonance lineshape calculated from 3D FEM for the mode at $L = 1547$ nm and $t = 0$ nm. The corresponding Q factor is about 26.43.

where m is a positive integer. Taking Eq. (8) into account, in Table 1, we list various parameters for two candidate mirror thicknesses $t = 0$ and 50 nm, at cavity lengths L around 0.6 and 1.5 μm, which satisfy the FP round-trip phase condition at $r = 70$ nm, $h = 10$ nm, and $n_c = 3.5$. We note that Ag mirrors with a thickness of 50 nm significantly increase the reflectivity (lower the mirror loss) when compared to the case of bare waveguide/air interfaces ($t = 0$).

To verify that Q_{FP} is a reasonable estimation of the Q factor for this plasmonic gap-mode nanocavity, we examine the mode at $L = 1547$ nm and $t = 0$ nm in Table 1 by carrying out 3D FEM calculations of the Q factor [28, 31]. We excite the cavity mode by a $\hat{y}$-polarized plane wave which has a wavelength-independent strength and is normally incident onto one Ag mirror from the free space outside the cavity. The spatial integration of the square magnitude $|\mathbf{E}(\mathbf{r})|^2$ of the electric field inside the gap region (proportional to the stored electric energy) is recorded as the wavelength is varied through the resonance. The Q factor is then calculated from the ratio between the full width at half maximum (FWHM) and resonance wavelength of the corresponding lineshape. The outcome is illustrated in Fig. 6. From the FWHM linewidth $\Delta\lambda \approx 58.9$ nm, the Q factor is around 26.43, which is in reasonable agreement with $Q_{FP} = 31.2$. We then look into the field profile of the high-Q mode at $L = 1511$ nm and $t = 50$ nm, which is potentially more promising for lasing than other modes. In Fig. 7, we illustrate the field profile excited by the $\hat{y}$-polarized plane wave at 1.55 μm. One can observe the subwavelength confinement of the plasmonic hybrid gap mode in the dielectric gap, as shown in Fig. 7(a). Due to the mode matching at the waveguide/mirror junction, the cross-sectional profile of the 3D mode pattern slightly deviates from that of the first-order mode in the infinitely long plasmonic waveguide. However,

#185769 - $15.00 USD Received 22 Feb 2013; revised 6 May 2013; accepted 21 May 2013; published 29 May 2013

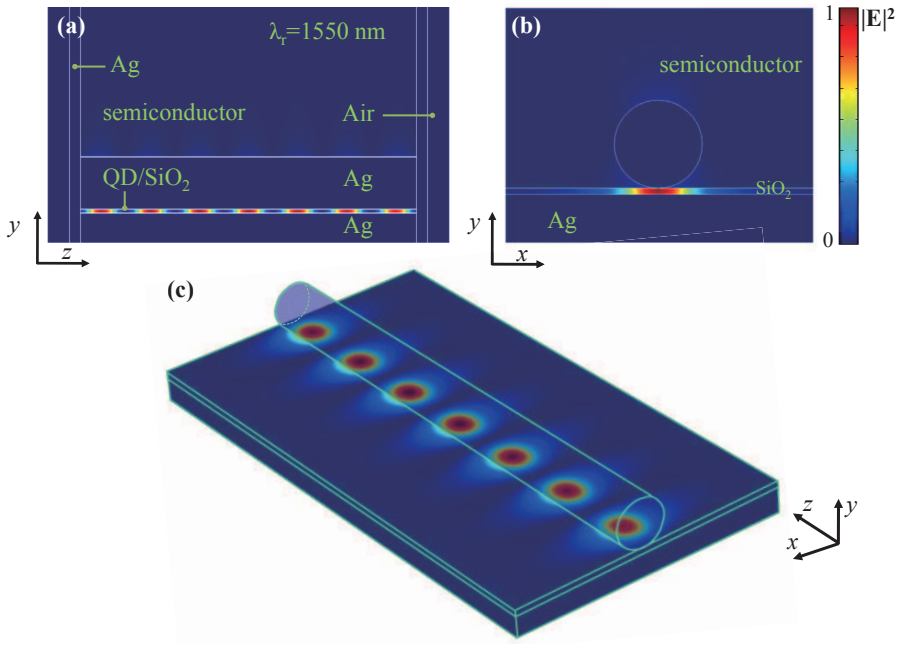

Fig. 7. (a) The side view (y-z plane), (b) front view (x-y plane), and (c) top (oblique) view (x-z plane) of the mode profile corresponding to the case of $L = 1511$ nm in Table 1. The field pattern is excited by a plane wave normally incident onto the Ag mirror from the free space outside the nanocavity.

these two cross-sectional profile resemble each other, as can be observed from Figs. 2(d) and 7(b). In fact, detailed comparisons reveal that not only the overall profile but also each Cartesian component of the two fields are similar to each other. This phenomenon indicates that the first-order mode is almost perfect for the mode matching at the waveguide/mirror junction. Therefore, estimations of reflection coefficients using the single-mode standing-wave pattern $|f(z)|$ in Eq. (6) should be quite accurate. Figure 7(c) shows the top (oblique) view of the mode profile below the nanowire. In addition to the clear standing-wave pattern along FP cavity (z direction), the mode is also laterally confined (x direction).

The threshold gains $g_{\mathrm{th,FP}}$ estimated from the FP formula in Table 1 are essential parameters of the nanolaser. As an independent check of these values, we incorporate a virtual gain (artificial and negative imaginary part of the permittivity of SiO_2) into the active region [38, 39] and carry out a frequency scanning of the field energy in the FP cavity by varying the wavelength of the incident plane wave around the resonance of 1.55 μm [28]. The obtained spectra would exhibit a very narrow lineshape (high *warm-cavity Q* factor) as the gain approaches the real threshold gain of the 3D cavity mode. The examinations indicate that the threshold gains obtained from the two approaches agree with each other.

From Table 1, the threshold gain $g_{\mathrm{th,FP}}$ of the cavity at $t = 50$ nm and $L = 625$ nm (2041.4 cm^{-1}) is still quite significant. Looking into the corresponding Q factor components Q_{abs} and Q_{mir}, we see that they are quite close. As Q_{abs} due to the absorption (206.0) cannot be altered much once the cross section of the waveguide is fixed, we need to increase Q_{mir} so that the threshold gain $g_{\mathrm{th,FP}}$ can drop even lower. By increasing the cavity length L to 1511 nm, which also supports the resonance at 1.55 μm, the component Q_{mir} (550.6) is enhanced and becomes larger than Q_{abs}. The Q factor at this longer cavity length exceeds 100, and the corresponding

#185769 - $15.00 USD Received 22 Feb 2013; revised 6 May 2013; accepted 21 May 2013; published 29 May 2013

threshold gain $g_{\mathrm{th,FP}}$ (1472.5 cm^{-1}) is lowered below 1500 cm^{-1}. This threshold gain may be sustainable by, for example, colloidal QDs such as PbS with intense optical pumping [23, 24].

5. Conclusion

We have analyzed a plasmonic gap-mode nanocavity at telecommunication wavelengths near 1.55 μm in high-index claddings such as semiconductors. In the high-index condition, the first-order mode of the plasmonic guiding structure exhibits the better field confinement in the active region than the fundamental one does and is therefore more promising for lasing. The advantage of the first-order mode is also reflected on its lower transparency threshold g_{tr} in this condition. We also study the dependence of the reflectivity on the thickness of the Ag reflector using the orthogonality theorem of waveguide modes and show that a decent reflectivity above 95 % is achievable with an Ag thickness of about a few tens of nanometers. This high reflectivity significantly lowers the mirror loss. For such cavities with a cavity length approaching 1.5 μm, a quality factor near 150 and threshold gain lower than 1500 cm^{-1} are achievable.

Acknowledgments

This work was sponsored by Research Center for Applied Sciences, Academia Sinica, Taiwan, and National Science Council, Taiwan, under Grant numbers NSC100-2112-M-001-002-MY2 and NSC-101-2218-E-019-002. The authors would also like to thank Professor Shun Lien Chuang at the Department of Electrical and Computer Engineering, University of Illinois at Urbana-Champaign, for his encouragements and fruitful discussions.

#185769 - $15.00 USD Received 22 Feb 2013; revised 6 May 2013; accepted 21 May 2013; published 29 May 2013